4

Parallel Shear Flow: the Effects of Stratification

The Earth's oceans and atmosphere tend to be inhomogeneous, with density differences that can strongly affect the motion. The primary reason for the inhomogeneity is heat radiation. At the equator, both ocean and atmosphere gain heat from the sun. Near the poles, the ocean loses heat to the atmosphere, while the atmosphere radiates heat into space at all latitudes. Ocean density is also governed by salinity. All of these processes create inhomogeneities which, under the action of gravity, tend to rearrange themselves into horizontal layers. We therefore say that these fluids are "density-stratified," or just "stratified." Based on our experience

Figure 4.1 Sunrise over Jonesport, Maine, showing Kelvin-Helmholtz billow clouds. Photo courtesy of Gene Hart.

https://doi.org/10.1017/9781108640084.005 Published online by Cambridge University Press

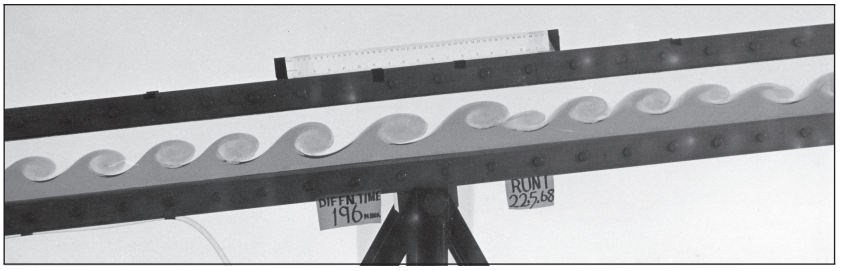

Figure 4.2 Kelvin-Helmholtz billows in a stratified laboratory flow (Thorpe, 1971). The tank is filled with a layer of pure water overlying a layer of denser salt water. When the tank is tilted, the dense lower layer flows downward, forcing the upper layer upward, resulting in an accelerating, stratified shear flow. Eventually, the shear becomes strong enough to overcome the stable stratification, and instability appears.

with motionless equilibria (Chapter 2) we call stratification "statically stable" when buoyant fluid overlies dense fluid. But if a shear flow is present, stability is less easy to predict.

When layers move relative to one another, there is the likelihood of shear instability, as we have seen (Chapter 3). But if the fluid is stably stratified, a growing perturbation (e.g., Figures 4.1 and 4.2) must expend some of its energy doing work against gravity. This tends to reduce the growth rate, and instability may be damped completely by sufficiently strong stratification. In some cases, though, statically stable stratification can interact with shear to create new mechanisms of instability that would not exist in a homogeneous shear flow.

In Figure 4.3, a shear layer is set up by the passage of an internal gravity wave. The wave rides on the slight difference in buoyancy between the surface water and the water below 20 m depth. Internal waves are big and slow: these ones have a period of 10 minutes and a wavelength of several hundred meters. Wave motion causes shear across the buoyancy interface. The shear is strongest on the upstream face of the wave, producing Kelvin-Helmholtz instability. The instability is powered by the shear and resisted by the buoyancy difference. Note, though, that the wave, and therefore the shear, would not exist without the buoyancy difference.

In Figure 4.4, observations at 550 m depth off the Canary Islands show a cold bottom layer where the speed of the tidal current drops to zero. The shear between the bottom layer and the warmer overlying ocean overcomes the buoyancy difference, resulting in Kelvin-Helmholtz instability. The same instability occurs in air, as made visible by the fog layer in Figure 4.5.

In this chapter we will explore stratification effects analytically, taking advantage of the relative simplicity of the inviscid equations. Numerical solution methods will be taken up in Chapter 6, after we have incorporated viscosity and diffusion.

https://doi.org/10.1017/9781108640084.005 Published online by Cambridge University Press

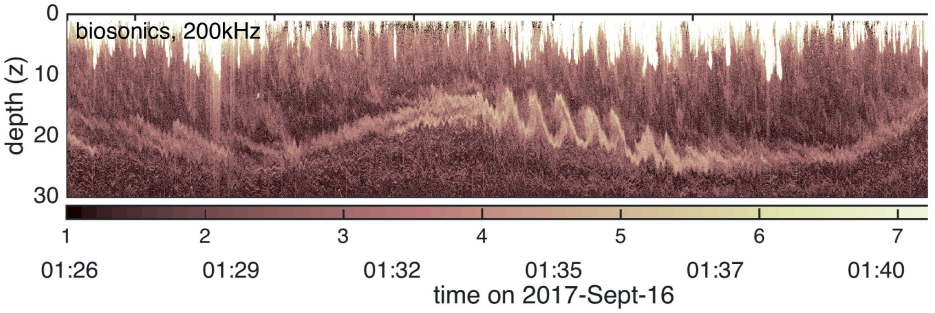

Figure 4.3 Echosounder image showing Kelvin-Helmholtz billows growing on an interfacial gravity wave off the California coast. The wave was visualized by a shipboard echosounder. Similar in principle to a medical ultrasound, it registers sound waves reflected from biota and from tiny changes in water density due to centimeter-scale turbulence. Image is courtesy of J. MacKinnon, J. Colosi, and A. Suanda.

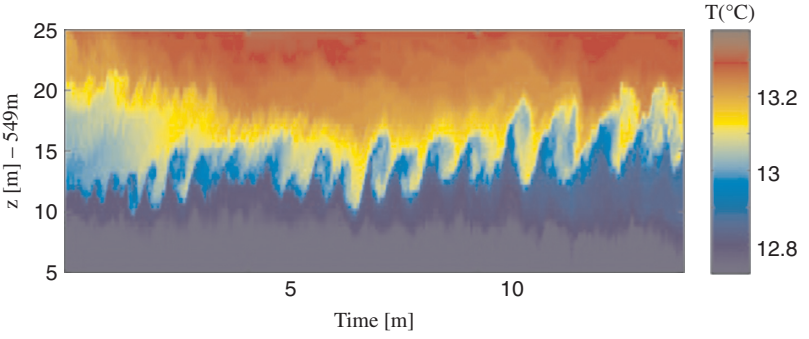

Figure 4.4 Temperature variations in a downslope tidal flow. This time series was constructed using data from multiple temperature sensors spaced vertically on a chain above the sea floor at 550 m depth. Typical wavelengths are inferred to be 75 m. Graphic courtesy H. van Haren (after Van Haren and Gostiaux, 2009).

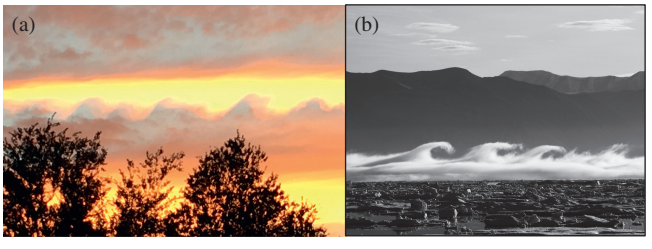

Figure 4.5 (a) Kelvin-Helmholtz instability in a stratified shear flow revealed by a cloud layer over Boston, MA. Photo courtesy of Alexis Kaminski. (b) Instability in a cold fog layer near Nares Strait in northern Canada. Photo courtesy Scott McAuliffe.

https://doi.org/10.1017/9781108640084.005 Published online by Cambridge University Press

4.1 The Richardson Number

A sheared flow has kinetic energy that can power the growth of an instability, as we saw in section 3.10, while statically stable stratification represents an energy *sink*, as a disturbance must do work against gravity in order to grow. On this basis, we may propose a provisional "rule of thumb" for stratified shear flows:

- $U_z \neq 0$ will tend to destabilize the flow, while
- $B_z > 0$ will tend to stabilize the flow.

We will find that, like all rules of thumb, this one is valid often enough to be useful, but can also be dead wrong.

To quantify the relationship between shear and stratification, we define the gradient Richardson number:

$$Ri = \frac{B_z}{U_z^2}. \tag{4.1}$$

[A more general definition, $Ri = B_z/(U_z^2 + V_z^2)$, allows for flow in any horizontal direction.] We can imagine two limiting cases:

- $Ri \gg 1$: stratification dominates, shear is weak, and we don't expect instability.
- $Ri \ll 1$: shear dominates, stratification is weak, and instability is therefore likely.

What do we expect at moderate values of Ri? Is there a critical value of Ri that separates stable and unstable regimes? The answer is yes, usually, but the critical value depends on the details of the flow geometry. We'll get into this later; for now, be content to know that the critical value is typically of order unity.

To illustrate, consider the hyperbolic tangent model for the stably stratified shear layer:

$$U = u_0 \tanh\frac{z}{h}\ ; \quad B = b_0 \tanh\frac{z}{h}. \tag{4.2}$$

Differentiating, we have

$$B_z = \frac{b_0}{h}\operatorname{sech}^2\frac{z}{h}\ ; \quad U_z^2 = \frac{u_0^2}{h^2}\operatorname{sech}^4\frac{z}{h}.$$

$$\Rightarrow \quad Ri = \frac{b_0 h}{u_0^2}\cosh^2\frac{z}{h}. \tag{4.3}$$

The profile is shown in Figure 4.6. It is often convenient to define a bulk Richardson number, Ri_b , whose value characterizes the shear flow as a whole. A natural choice is the coefficient $b_0 h/u_0^2$, which in this case is also the minimum value of $Ri(z)$. We will find in section 4.4 that this flow is unstable if and only if $Ri_b < 1/4$.

https://doi.org/10.1017/9781108640084.005 Published online by Cambridge University Press

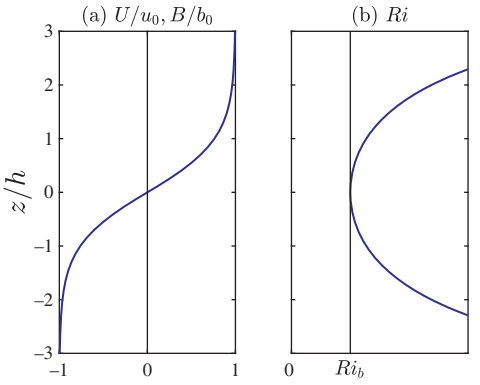

Figure 4.6 (a) Velocity/buoyancy profile for the hyperbolic tangent stratified shear layer (4.2). (b) Gradient Richardson number profile. The vertical line indicates the bulk Richardson number.

4.2 Equilibria and Perturbations

To derive the perturbation theory for stratified, parallel shear flows, we start with the Boussinesq equations for an inviscid, nondiffusive, inhomogeneous fluid. We ignore planetary rotation. The divergence equation is, as usual,

$$\vec{\nabla} \cdot \vec{u} = 0.$$

The momentum equation (1.19), neglecting the Coriolis acceleration and viscosity but restoring buoyancy, is

$$\frac{D\vec{u}}{Dt} = -\vec{\nabla}\pi + b\hat{e}^{(z)}, \tag{4.4}$$

and the buoyancy equation (1.25) is

$$\frac{Db}{Dt} = 0. \tag{4.5}$$

We assume the perturbation solution

$$\begin{aligned} \vec{u} &= U(z)\hat{e}^{(x)} + \epsilon\vec{u}', \\ b &= B(z) + \epsilon b', \\ \pi &= \Pi + \epsilon\pi'. \end{aligned} \tag{4.6}$$

No assumption is made regarding the background pressure Π. As always, the perturbation velocity has zero divergence: $\vec{\nabla} \cdot \vec{u}' = 0$.

Substituting (4.6) into the momentum equation (4.4) gives

https://doi.org/10.1017/9781108640084.005 Published online by Cambridge University Press

$$\left[\frac{\partial}{\partial t}+U\frac{\partial}{\partial x}+\varepsilon\vec{u}'\cdot\vec{\nabla}\right]\left[U(z,t)\hat{e}^{(x)}+\varepsilon\vec{u}'\right]=-\vec{\nabla}\left[\Pi+\varepsilon\pi'\right]+\left[B(z,t)+\varepsilon b'\right]\hat{e}^{(z)} \tag{4.7}$$

With no perturbation ($\epsilon = 0$), this gives

$$\vec{\nabla}\Pi = B\hat{e}^{(z)},$$

i.e., the background pressure varies only in the vertical, where it maintains hydrostatic balance with the background buoyancy.

The $O(\epsilon)$ terms in (4.7) give

$$\left(\frac{\partial}{\partial t}+U\frac{\partial}{\partial x}\right)\vec{u}'+U_z w'\hat{e}^{(x)}=-\vec{\nabla}\pi'+b'\hat{e}^{(z)}. \tag{4.8}$$

This is the same as the homogeneous case (3.7) except for the second term on the right-hand side, which describes vertical accelerations due to the perturbation buoyancy.

Substitution of (4.6) into (4.5) gives

$$\left[\frac{\partial}{\partial t}+U\frac{\partial}{\partial x}+\varepsilon\vec{u}'\cdot\vec{\nabla}\right]\left[B(z)+\varepsilon b'\right]=0. \tag{4.9}$$

For $\epsilon = 0$, this gives $0 = 0$, so there is no restriction on the background buoyancy profile. The $O(\epsilon)$ part of (4.9) is:

$$\left(\frac{\partial}{\partial t}+U\frac{\partial}{\partial x}\right)b'+B_z w'=0. \tag{4.10}$$

It is worthwhile to compare (4.10) with (2.12), the equation for buoyancy perturbations from hydrostatic equilibrium in a motionless, stratified fluid. The final term on the left-hand side describes the advection of the background buoyancy gradient by the vertical velocity perturbation, just as we saw in (2.12). The second term on the left-hand side is new; it describes the advection of buoyancy perturbations by the background flow (which was zero in the motionless case).

4.2.1 Eliminating the Pressure

We eliminate the pressure, as we have done before, by combining the divergence of the momentum equation (4.8) with the Laplacian of its vertical component. The divergence gives a Poisson equation for the pressure:[1]

$$\nabla^2\pi' = -2U_z\frac{\partial w'}{\partial x}+\frac{\partial b'}{\partial z}. \tag{4.11}$$

[1] Compare this with equations (2.16) and (3.11).

https://doi.org/10.1017/9781108640084.005 Published online by Cambridge University Press

The vertical component of (4.8) is

$$\left(\frac{\partial}{\partial t} + U\frac{\partial}{\partial x}\right) w' = -\frac{\partial \pi'}{\partial z} + b'. \tag{4.12}$$

Finally, we take the Laplacian of (4.12) and substitute the vertical derivative of (4.11) to obtain:

$$\left(\frac{\partial}{\partial t} + U\frac{\partial}{\partial x}\right) \nabla^2 w' - U_{zz}\frac{\partial w'}{\partial x} = \nabla_H^2 b'. \tag{4.13}$$

In (4.13) and (4.10), we have two equations for the two unknowns w' and b'. We substitute the normal mode forms $w' = \{\hat{w}(z)e^{\sigma t}e^{\imath(kx+\ell y)}\}_r$ and $b' = \{\hat{b}(z)e^{\sigma t}e^{\imath(kx+\ell y)}\}_r$ to obtain a pair of ordinary differential equations:

$$(\sigma + \imath kU)\nabla^2\hat{w} - \imath kU_{zz}\hat{w} = -\tilde{k}^2\hat{b} \tag{4.14}$$

$$(\sigma + \imath kU)\hat{b} + B_z\hat{w} = 0, \tag{4.15}$$

where $\nabla^2 = d^2/dz^2 - \tilde{k}^2$.

4.3 Oblique Modes

Here we will look at obliquity effects using two kinds of Squire transformations. First we extend the approach used previously in section 3.7. We then introduce a new approach based on transforming the velocity profile.

4.3.1 Transforming the Buoyancy

Consider an oblique mode that obeys the equations derived above for stratified shear flow:

$$(\sigma + \imath kU)\nabla^2\hat{w} - \imath kU_{zz}\hat{w} = -\tilde{k}^2\hat{b} \tag{3D1}$$

$$(\sigma + \imath kU)\hat{b} + B_z\hat{w} = 0, \tag{3D2}$$

where

$$\nabla^2 = \frac{d^2}{dz^2} - \tilde{k}^2\ ; \quad \tilde{k} = \sqrt{k^2 + \ell^2}.$$

Suppose also that we have a solution algorithm

$$\sigma = \mathcal{F}(z, U, B_z;\ k, \ell).$$

The corresponding 2D mode with wave vector $(\tilde{k}, 0)$ obeys:

$$(\sigma + \imath\tilde{k}U)\nabla^2\hat{w} - \imath\tilde{k}U_{zz}\hat{w} = -\tilde{k}^2\hat{b} \tag{2D1}$$

https://doi.org/10.1017/9781108640084.005 Published online by Cambridge University Press

$$(\sigma + \imath\tilde{k}U)\hat{b} + B_z\hat{w} = 0, \tag{2D2}$$

and therefore has the solution algorithm $\sigma_{2D} = F(z, U, B_z;\ \tilde{k}, 0)$.

Is there a transformation that makes these $(2D)$ equations isomorphic with the $(3D)$? We begin by defining the Squire transformations

$$\sigma = \cos\varphi\ \tilde{\sigma}; \quad \hat{b} = \cos\varphi\ \tilde{\hat{b}}.$$

Now substitute these into $(3D1)$ and divide out the common factor $\cos\varphi$. The result is isomorphic to $(2D1)$

$$(\tilde{\sigma} + \imath\tilde{k}U)\nabla^2\hat{w} - \imath\tilde{k}U_{zz}\hat{w} = -\tilde{k}^2\tilde{\hat{b}}. \tag{$\widetilde{3D1}$}$$

Turning to equations $(3D2)$ and $(2D2)$, we now define the additional transformation

$$B_z = \cos^2\varphi\ \tilde{B}_z.$$

Substituting into $(3D2)$ and dividing out $\cos^2\varphi$, we obtain:

$$(\tilde{\sigma} + \imath\tilde{k}U)\tilde{\hat{b}} + \tilde{B}_z\hat{w} = 0. \tag{$\widetilde{3D2}$}$$

With these transformations, $(\widetilde{3D1})$ and $(\widetilde{3D2})$ are isomorphic to $(2D1)$ and $(2D2)$, respectively, and can therefore be solved using the same solution algorithm: $\tilde{\sigma} = \mathcal{F}(z, U, \tilde{B}_z;\ \tilde{k}, 0)$, or

$$\sigma_{3D} = \cos\varphi \times \mathcal{F}\left(z, U, \frac{B_z}{\cos^2\varphi};\ \tilde{k}, 0\right).$$

The growth rate of the 3D mode is $\cos\varphi$ times that of a corresponding 2D mode that exists *in a fluid with stronger stratification*. In most circumstances this means that the oblique mode will have a slower growth rate, but if stratification should somehow increase the growth rate, and do so rapidly enough to compensate for the obliquity factor $\cos\varphi$, then the oblique mode may grow faster.

Since the angle of obliquity enters only through the function $\cos\varphi$, its sign is irrelevant. Oblique modes therefore come in pairs, identical in every respect except the sign of φ. Such a pair, growing at the same rate, forms a criss-crossing pattern of crests and troughs.

4.3.2 Transforming the Background Velocity

A normal mode perturbation in a shear flow is affected only by the component of the background flow that is parallel to its own wave vector. To see this, inspect (4.14) and (4.15) and note that, wherever U appears, it is multiplied by k. If we

https://doi.org/10.1017/9781108640084.005 Published online by Cambridge University Press

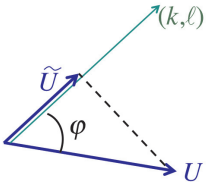

Figure 4.7 Definition sketch for $\tilde{U}$, the component of the background current U in the direction of the wave vector (k, ℓ).

define $\tilde{U}$ such that $kU = \tilde{k}\tilde{U}$ and substitute, we get a pair of equations that is isomorphic to the 2D case with wave vector $(\tilde{k}, 0)$:

$$(\sigma + \imath\tilde{k}\tilde{U})\nabla^2\hat{w} - \imath\tilde{k}\tilde{U}_{zz}\hat{w} = -\tilde{k}^2\hat{b}$$
$$(\sigma + \imath\tilde{k}\tilde{U})\hat{b} + B_z\hat{w} = 0.$$

In fact, the profile $\tilde{U}$ that we just defined is the component of U parallel to the wave vector:

$$\boxed{\tilde{U} = \frac{k}{\tilde{k}}U = U\cos\varphi,}$$

as illustrated in Figure 4.7. So if the growth rate is given by a solution algorithm

$$\sigma = \mathcal{F}(z, U, B_z;\ k, l),$$

then it is also true that

$$\sigma = \mathcal{F}(z, \tilde{U}, B_z;\ \tilde{k}, 0).$$

4.4 The Taylor-Goldstein Equation

Based on the results of the previous two sections, we restrict our attention to 2D modes. Replacing $\tilde{k}$ with k, (4.14) and (4.15) become

$$(\sigma + \imath kU)\left(\frac{d^2}{dz^2} - k^2\right)\hat{w} - \imath kU_{zz}\hat{w} = -k^2\hat{b} \tag{4.16}$$
$$(\sigma + \imath kU)\hat{b} + B_z\hat{w} = 0. \tag{4.17}$$

If we should need to apply these results to a 3D mode, we simply replace U by $\tilde{U}$ as defined in (4.3.2).

We can derive a single equation for $\hat{w}$ by solving (4.17) for $\hat{b}$ and substituting into (4.16), giving

$$(\sigma + \imath kU)\left(\frac{d^2}{dz^2} - k^2\right)\hat{w} - \imath kU_{zz}\hat{w} = k^2\frac{B_z\hat{w}}{(\sigma + \imath kU)}.$$

https://doi.org/10.1017/9781108640084.005 Published online by Cambridge University Press

Finally, we substitute $\sigma = -\imath kc$ and rearrange to obtain the Taylor-Goldstein (TG) equation:

$$\boxed{\hat{w}_{zz} + \left\{ \frac{B_z}{(U-c)^2} - \frac{U_{zz}}{U-c} - k^2 \right\} \hat{w} = 0.} \tag{4.18}$$

Note that Rayleigh's equation (3.19) can be recovered by setting $B_z = 0$.

Exercise: If you're good with hyperbolic functions (or want to be), try this. Consider the hyperbolic tangent profiles (4.2). Nondimensionalize the problem using the shear scaling, with velocity scale u_0 and length scale h, so that

$$U_\star = \tanh z_\star \; ; \qquad B_\star = Ri_b \tanh z_\star. \tag{4.19}$$

and $k^\star = kh$. Now suppose that, when Ri_b is not too large, there is a stationary instability like the one we found in the unstratified case (section 3.9.1). Assume also that, if Ri_b is made sufficiently large, the instability is quenched so that $c_\star = 0$. How large must Ri_b be? Try this solution:

$$\hat{w}_\star = (\operatorname{sech} z_\star)^{k_\star} |\tanh z_\star|^{(1-k_\star)}.$$

After a half hour or so of differentiating, you should find that this solution works provided that

$$Ri_b = k_\star(1 - k_\star).$$

This tells us that the stability boundary is an inverted parabola on the $k_\star - Ri_b$ plane with peak at $k_\star = 1/2$, $Ri_b = 1/4$ (illustrated later on figure 6.3). In other words, the critical Richardson number for this flow is 1/4.

Also, as this critical Richardson number is approached, the wavenumber of the fastest-growing mode approaches 1/2, not very different from the value 0.44 found in the unstratified case. More precisely, the ratio of wavelength $2\pi/k$ to shear layer thickness $2h$ approaches 2π, whereas in the homogeneous case the value is 7. In the context of a "rule of thumb," these two values are effectively equal.

4.5 Application to Internal Wave Phenomena

Solutions of (4.18) with real c represent waves: internal gravity waves (section 2.2.1), vorticity waves (section 3.12.2), or some combination of the two. If we set $U = 0$ and $B_z =$ constant in (4.18), we recover the dispersion relation for internal gravity waves in uniform stratification (section 2.2.1).

The limit $k \to 0$ is called the hydrostatic limit. Near that limit, perturbations involve very weak vertical accelerations and are therefore nearly in hydrostatic

https://doi.org/10.1017/9781108640084.005 Published online by Cambridge University Press

balance (like the background flow). If we take this limit and also assume $U = 0$, the TG equation becomes

$$\hat{w}_{zz} + \frac{B_z}{c^2}\,\hat{w} = 0.$$

This is the equation for baroclinic normal modes, whose description may be found in any geophysical fluid dynamics text. The hydrostatic limit is a useful description not only for small-amplitude waves but also for nonlinear phenomena such as solitary waves, bores, hydraulic jumps, and gravity currents. For example, in the weakly nonlinear theory of solitary waves in a stratified shear flow, the dependence on x and t is described by the Korteweg-De Vries equation, while the vertical structure is a solution of the TG equation (4.18) in the hydrostatic limit (Lee and Beardsley, 1974).

Although we will not venture far into the realm of waves here, it is important to note that *the numerical methods that we are developing (sections 3.5, 6.2) apply just as well to waves as they do to instabilities.* Those methods are often used to determine gravity wave and baroclinic mode characteristics in realistic situations where the stratification is not uniform and the background current is nonzero.

4.6 Analytical Examples of Instability in Stratified Shear Flows

Like the Rayleigh equation (3.16–3.19), the TG equation (4.18) is easy to solve when the background profiles are sufficiently simple. Here we describe a few examples that show how shear instability is affected by stratification.

4.6.1 Kelvin-Helmholtz and Rayleigh-Taylor Instabilities at an Interface

Imagine an infinitely thin interface at which the velocity and the buoyancy change:

$$U = \frac{\Delta u}{2}\begin{cases} 1, & z > 0 \\ -1, & z < 0 \end{cases} \qquad B = \frac{\Delta b}{2}\begin{cases} 1, & z > 0 \\ -1, & z < 0 \end{cases} \tag{4.20}$$

As expressed in (4.18), the TG equation involves the second-derivative U_{zz} and therefore cannot handle this discontinuity in U. To get around this problem we rephrase the TG equation in terms of the vertical displacement function η', defined by

$$w' = \left(\frac{\partial}{\partial t} + U\frac{\partial}{\partial x}\right)\eta'.$$

In normal mode form this is

$$\hat{w} = (\sigma + \imath k U)\hat{\eta} = \imath k(U - c)\hat{\eta}.$$

https://doi.org/10.1017/9781108640084.005 Published online by Cambridge University Press

With this change of variables (4.18) becomes

$$\left[(U-c)^2\hat{\eta}_z\right]_z + \left[B_z - k^2(U-c)^2\right]\hat{\eta} = 0. \tag{4.21}$$

(You will derive this in homework problem 9.)

The solution is simple because U and B are constant except at the interface. Requiring that $\hat{\eta}$ be continuous and bounded for all z and assuming $k > 0$,

$$\hat{\eta} = Ae^{-k|z|}. \tag{4.22}$$

The discontinuity in $B(z)$ imposes another condition on the solution. Because of that discontinuity, the derivative B_z has the form of a Dirac delta function (section 2.2.4):

$$B_z = \Delta b\,\delta(z). \tag{4.23}$$

Using property 3 of the delta function (listed in Figure 2.5), you can check that (4.23) integrates to give $B(z)$ as defined in (4.20).

We now apply the integral operation $\lim_{\epsilon\to 0}\int_{-\epsilon}^{\epsilon} dz$ to (4.21). The first term gives

$$\lim_{\epsilon\to 0}\int_{-\epsilon}^{\epsilon}\left[(U-c)^2\hat{\eta}_z\right]_z dz \;=\; \left[\left[(U-c)^2\hat{\eta}_z\right]\right]_0.$$

Next,

$$\lim_{\epsilon\to 0}\int_{-\epsilon}^{\epsilon} B_z\hat{\eta}\,dz \;=\; \lim_{\epsilon\to 0}\int_{-\epsilon}^{\epsilon}\Delta b\,\delta(z)\;\hat{\eta}\,dz \;=\; \Delta b\hat{\eta}(0),$$

where property 5 of the delta function has been used. The final term is

$$\lim_{\epsilon\to 0}\int_{-\epsilon}^{\epsilon}\left[k^2(U-c)^2\hat{\eta}\right]dz \;=\; 0.$$

This integral vanishes because the integrand is finite, so when we take the limit $\epsilon \to 0$ the result is zero. Summing these three integrated terms, we have a combined jump condition for a buoyancy change and a velocity change:

$$\boxed{\left[\left[(U-c)^2\hat{\eta}_z\right]\right]_0 + \Delta b\hat{\eta}(0) = 0.} \tag{4.24}$$

Exercise: Starting from (4.24) recover (2.41), the jump condition for a buoyancy interface in a motionless fluid, by making the appropriate substitutions.

Substituting from (4.22), (4.24) becomes

$$-k\left[\left(\frac{\Delta u}{2}-c\right)^2 + \left(-\frac{\Delta u}{2}-c\right)^2\right] + \Delta b = 0. \tag{4.25}$$

which we can solve for c to get

$$c = \pm\sqrt{\frac{\Delta b}{k} - \frac{\Delta u^2}{4}}.$$

https://doi.org/10.1017/9781108640084.005 Published online by Cambridge University Press

or

$$\sigma = \pm\sqrt{\frac{\Delta u^2}{4}k^2 - \Delta b k}.$$

Evidently Δu has a destabilizing effect regardless of its sign, whereas positive Δb acts to reduce the growth rate. (Remember we have assumed that $k > 0$.)

In terms of the nondimensional variables

$$c^\star = \frac{c}{\Delta u}\,; \quad k^\star = k\frac{\Delta u^2}{\Delta b}\,; \quad \sigma^\star = \frac{\Delta u}{\Delta b}\sigma$$

the dispersion relations become

$$\boxed{c^\star = \pm\sqrt{\frac{1}{k^\star} - \frac{1}{4}}\,; \quad \sigma^\star = \mp\sqrt{\frac{k^{\star 2}}{4} - k^\star}}$$

If $0 \le k^\star \le 4$, $c^\star$ is real and the solution describes two waves moving oppositely (Figure 4.8; blue curves). Otherwise, if $k^\star > 4$ or $k^\star < 0$ (which corresponds to $\Delta b < 0$), we have a growing and a decaying mode (red curves).

- As long as $\Delta u \neq 0$, the flow is unstable, i.e., there is always a range of k in which one solution has $\sigma_r > 0$. These provide the simplest example of the Kelvin-Helmholtz instability: a shear instability partially damped by stable stratification.
- The instability exhibits ultraviolet catastrophe: the shortest waves (largest $k^\star$) have arbitrarily large growth rate.
- Modes with $0 \le k^\star \le 4$ represent interfacial waves.

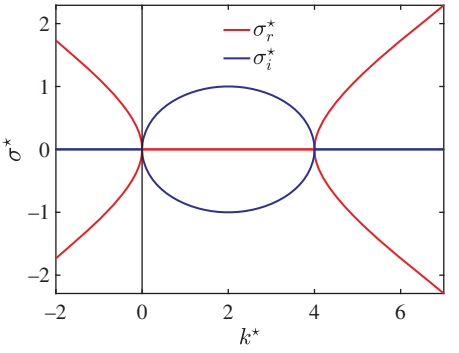

Figure 4.8 Waves and instabilities on a sharp interface at which velocity and buoyancy change discontinuously (4.20). The scaled wavenumber and growth rate are defined as $k^\star = ku_0^2/b_0$ and $\sigma^\star = \sigma u_0/b_0$, respectively.

https://doi.org/10.1017/9781108640084.005 Published online by Cambridge University Press

- If the buoyancy change is *unstable* ($\Delta b < 0$), then the scaled wavenumber is negative (though the dimensional wavenumber is not). The interface is convectively unstable, and all disturbances are amplified. This is a generalization of the Rayleigh-Taylor instability that we explored in section 2.2.4.

4.6.2 The Stratified Shear Layer

The previous example can be made more realistic by considering a shear layer with finite thickness $2h$, as in section 3.3, but retaining the two-layer stratification profile:

$$U(z) = u_0 \begin{cases} 1, & z \geq h \\ z/h, & -h < z < h \\ -1, & z \leq -h \end{cases} \quad \text{and} \quad B(z) = b_0 \begin{cases} 1, & z > 0 \\ 0, & z < 0. \end{cases} \tag{4.26}$$

The Taylor-Goldstein equation (4.18) simplifies considerably, permitting an analytical solution. This is due to the delta function behavior of the vorticity and buoyancy gradient profiles, viz.,

$$U_{zz}(z) = \Delta Q_1 \delta(z-h) + \Delta Q_2 \delta(z+h) \quad \text{and} \quad B_z(z) = b_0 \delta(z), \tag{4.27}$$

where $\Delta Q_1 = -u_0/h$ and $\Delta Q_2 = u_0/h$. In the regions between the interfaces of the flow, where the delta functions in (4.27) are centered, (4.18) reduces to

$$\hat{w}_{zz} - k^2 \hat{w} = 0. \tag{4.28}$$

Requiring that $\hat{w}$ be (first) continuous across each interface and (second) bounded as $z \to \pm\infty$, we can write the solution as

$$\hat{w}(z) = A_0 e^{-k|z|} + A_1 e^{-k|z-h|} + A_2 e^{-k|z+h|}, \tag{4.29}$$

where the A_i are constants to be determined and k is assumed to be positive. Note that this solution is similar to the piecewise shear layer of section 3.3, in that each interface has its own "influence" function associated with it, which decays exponentially over a vertical scale of k^{-1}. The only difference is that we now have a buoyancy interface (with coefficient A_0) in addition to the two vorticity interfaces with coefficients A_1 (upper) and A_2 (lower).

Values of the coefficients are found by applying a jump condition at each interface. We'll do this first for a *general* interface, located at z_j and allowing for *both* a vorticity jump ΔQ_j and a buoyancy jump Δb_j.

General Jump Condition

Multiplying the Taylor-Goldstein equation (4.18) by $(U-c)^2$, and integrating across a small region encompassing an interface at z_j gives

https://doi.org/10.1017/9781108640084.005 Published online by Cambridge University Press

$$\lim_{\epsilon\to 0}\int_{z_j-\epsilon}^{z_j+\epsilon}\Big[(U-c)^2\hat{w}_{zz}-U_{zz}(U-c)\hat{w}+B_z\hat{w}-k^2(U-c)^2\hat{w}\Big]dz=0. \quad (4.30)$$

The first term is integrated by parts to give $\big[\!\big[(U-c)^2\hat{w}_z\big]\!\big]_j$. Because $(U-c)^2$ is continuous, this is equivalent to $(U-c)^2\big[\!\big[\hat{w}_z\big]\!\big]_j$. The second and third terms of (4.30) can be evaluated directly using the properties of delta functions (Figure 2.5), and the last term vanishes as $\epsilon\to 0$. We now have the general jump condition at an interface with a buoyancy jump Δb_j and/or a vorticity jump ΔQ_j:

$$\boxed{(U_j-c)^2\big[\!\big[\hat{w}_z\big]\!\big]_j-\Delta Q_j(U_j-c)\hat{w}_j+\Delta b_j\hat{w}_j=0} \quad (4.31)$$

where the j subscripts indicate that the function is evaluated at z_j, e.g., $U_j=U(z_j)$. Exercise: Check that, for the special case of a vorticity jump in a homogeneous environment, $\Delta b_j=0$, (4.31) reproduces the previous result (3.30). Verify also that, for a buoyancy jump only, (4.31) is equivalent to (4.24) with U continuous and also to (2.41).

We now apply (4.31) at the three interfaces in turn.

- For the interface at $z=h$, $\hat{w}=A_0e^{-|kh|}+A_1+A_2e^{-2|kh|}$, $\big[\!\big[\hat{w}_z\big]\!\big]=-2kA_1$, $U=u_0$, the vorticity jump is $\Delta Q_1=-u_0/h$, and $\Delta b=0$. Substituting these expressions into (4.31) gives

$$\Big(u_0-c\Big)A_1+\frac{\Delta Q_1}{2k}\Big(A_0e^{-kh}+A_1+A_2e^{-2kh}\Big)=0. \quad (4.32)$$

- Similarly, applying (4.31) at $z=-h$ gives

$$\Big(-u_0-c\Big)A_2+\frac{\Delta Q_2}{2k}\Big(A_0e^{-kh}+A_1e^{-2kh}+A_2\Big)=0. \quad (4.33)$$

- At the buoyancy interface $z=0$, we have $\Delta Q=0$, $\big[\!\big[\hat{w}_z\big]\!\big]=-2kA_0$, and $U=0$, so the jump condition results in

$$A_0c^2-\frac{b_0}{2k}(A_0+A_1e^{-kh}+A_2e^{-kh})=0. \quad (4.34)$$

Combining (4.32, 4.33, 4.34) results in a solution for A_0, A_1, and A_2 and a dispersion relation that is quadratic in c^2:

$$c^4+B_2c^2+B_0=0, \quad (4.35)$$

with coefficients

https://doi.org/10.1017/9781108640084.005 Published online by Cambridge University Press

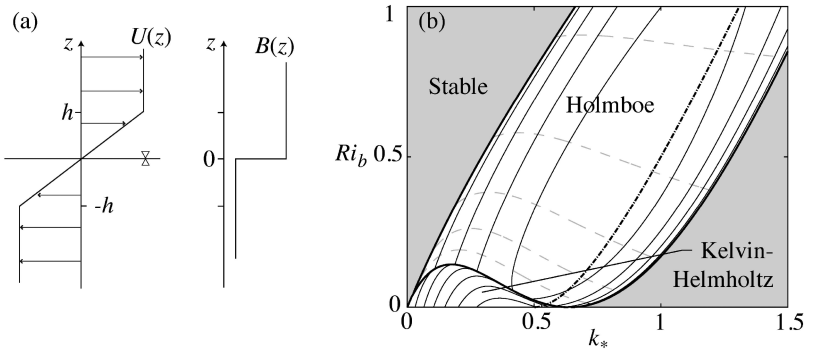

Figure 4.9 (a) Profiles of the piecewise stratified shear layer. The pair of triangles indicates the buoyancy interface. (b) Stability diagram of the piecewise stratified shear layer. Solid contours are of growth rate (every $0.03u_0/h$), and dashed gray contours are of phase speed (every $0.1u_0$), with gray representing stable regions of propagating waves. The resonance approximation from (4.39) is shown as a dash-dot line. Adapted from Carpenter et al. (2013).

$$B_2 = -[(u_0 + c_v)^2 + c_g^2 - c_v^2 e^{-4kh}]$$
$$B_0 = c_g^2\{(u_0 + c_v)^2 - e^{-2kh}[2(u_0 + c_v)c_v - c_v^2 e^{-2kh}]\}.$$

Here we have defined $c_v = \Delta Q_1/2k = -\Delta Q_2/2k$ and $c_g^2 = b_0/2k$, the intrinsic phase speeds of isolated vorticity and interfacial gravity waves as given in (2.44) and (3.81), respectively.

With the shear scaling $c_\star = c/u_0$, $k_\star = kh$ (cf. section 3.6), the dispersion relation has the form $c_\star(k_\star, Ri_b)$, where $Ri_b = b_0 h/u_0^2$ is a bulk Richardson number. The results of the stability analysis can therefore be plotted on the Ri_b-$k_\star$ plane, as shown in Figure 4.9. This diagram includes contours of growth rate $\sigma_r^\star$ (solid curves) and phase speed $c_r^\star$ (dashed), for the fastest-growing mode at each location on the plane.

For Ri_b less than about 0.07, there is a range of wavenumbers for which the growth rate is real and positive. At $Ri_b = 0$, this unstable regime extends from $k_\star = 0$ to $k_\star = 0.64$. This is the stratified extension of the shear instability described in section 3.3. As in that case, the instability has zero phase speed (i.e., moves with the mean flow speed) in this region. The instability is referred to as Kelvin-Helmholtz, as in section (4.6.1). As Ri_b is increased, the growth rate of the instability is reduced and the band of wavenumbers it occupies shrinks to zero. This is just as we would expect given that a growing mode must do work against gravity.

When Ri_b exceeds 0.07, the Kelvin-Helmholtz instability disappears, but the flow is *not* stable. Instead, a fundamentally different instability is found, the Holmboe instability. This instability is oscillatory; the fastest-growing mode is

https://doi.org/10.1017/9781108640084.005 Published online by Cambridge University Press

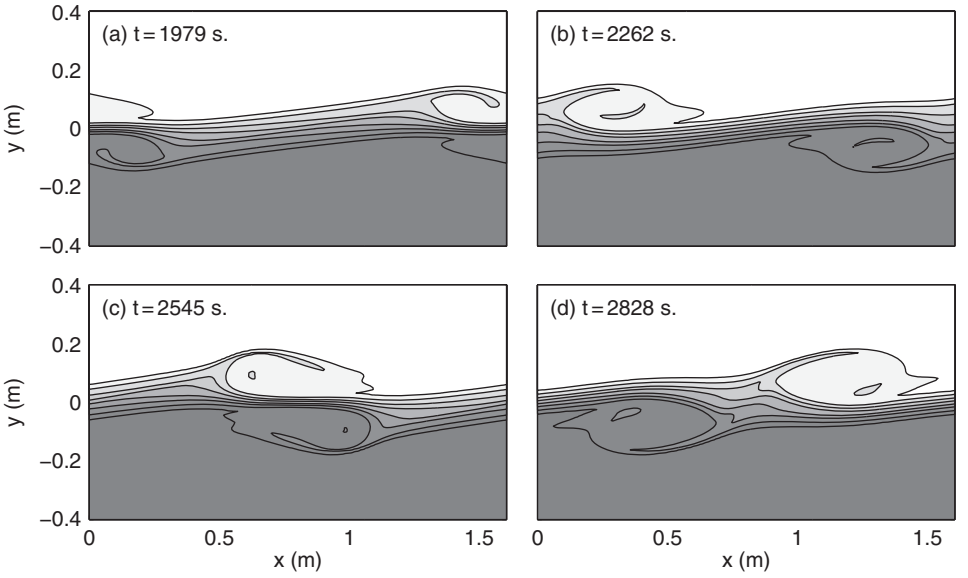

Figure 4.10 Buoyancy contours in a finite-amplitude Holmboe wave. Boundary conditions are horizontally periodic, so that each vortex is one member of an infinite sequence. Parameter values are $Ri_0 = 0.45$; $Re = 300$; $Pr = 9$; $k^\star = 0.35$; $\ell^\star = 0$ (from Smyth and Winters, 2003).

actually two modes with the same growth rate and equal but opposite phase speeds, one stronger in the upper half of the shear layer, the other in the lower half. This behavior is illustrated in Figure 4.10, which shows snapshots from a simulation of the nonlinear wave that grows from Holmboe instability. Each mode grows to form a finite-amplitude vortex. In Figure 4.10(a), the vortices are at the phase of maximal separation. The vortices approach (b), pass each other (c), and move apart (d).

Counterintuitively, the Holmboe instability exists *only* in the presence of statically stable stratification, and its growth rate increases with increasing Ri_b to a maximum at $Ri_b = 0.4$ (Figure 4.9b). To better understand the origin of the Holmboe instability, we look next at a simpler version of the piecewise stratified shear layer first proposed by Baines and Mitsudera (1994).

4.6.3 Holmboe Instability in a Semi-Infinite Shear Layer

Consider the same profiles as in Figure 4.9(a), except now we will remove the lower kink in $U(z)$, so that the shear extends infinitely toward negative z, as shown in Figure 4.11(a). The dispersion relation for this new set of profiles can be easily recovered by setting $A_2 = 0$ in (4.32, 4.34) and discarding (4.33). The result is a cubic equation for c,

https://doi.org/10.1017/9781108640084.005 Published online by Cambridge University Press

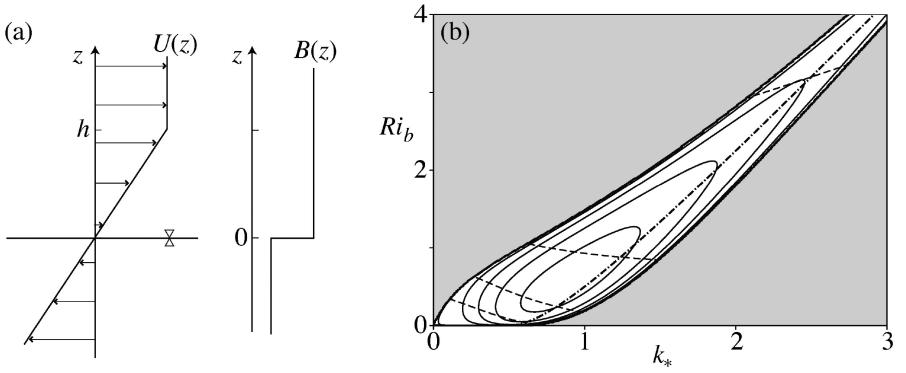

Figure 4.11 (a) Profiles illustrating the simplified setup for Holmboe's instability. (b) Stability characteristics of the Holmboe instability. Solid contours are of growth rate (every $0.03u_0/h$) with gray representing stable regions of propagating waves. All unstable modes are propagating with $c_r \neq 0$ and dashed contours spaced at $0.2u_0$. The resonance approximation from (4.39) is shown as a dash-dot line. Adapted from Baines and Mitsudera (1994) and Carpenter et al. (2013).

$$c^3 - (u_0 + c_v)c^2 - c_g^2 c - c_g^2[u_0 + c_v(1 - e^{-2kh})] = 0, \tag{4.36}$$

with c_v and c_g defined as above. Again we nondimensionalize and plot contours of growth rate, $\sigma_\star = k_\star c_i^\star$, on the $k_\star$-Ri_b plane in Figure 4.11(b).

The resulting stability diagram does not include a Kelvin-Helmholtz instability region, but displays the Holmboe instability with little alteration. Evidently the lower vorticity interface is crucial for the Kelvin-Helmholtz instability, but unnecessary for the Holmboe instability. This result can be understood when considering the Kelvin-Helmholtz instability to be an extension of the inflectional instability of the homogeneous piecewise shear layer, which relies on the interaction of vorticity waves at the upper and lower vorticity interfaces (section 3.12.3). By removing the inflection point (i.e., without the lower vorticity jump there is no change in the sign of U_{zz}) we have effectively eliminated this instability.

With the addition of a statically stable interface, we have generated a new instability. This is an example of how statically stable stratification can *destabilize* an otherwise stable flow, and is therefore a counterexample to our provisional "rule of thumb" suggested in section 4.1.

The origin of the Holmboe instability can be understood by considering the stable wave modes that are present in this system, and how they may interact to produce instability (as discussed in section 3.12 for homogeneous shear flows). The phase speeds of these wave modes are shown in Figure 4.12 for the example $Ri_b = 2$. Three modes can be identified: the vorticity wave and two internal gravity waves that propagate on the buoyancy interface in opposite directions. The phase

https://doi.org/10.1017/9781108640084.005 Published online by Cambridge University Press

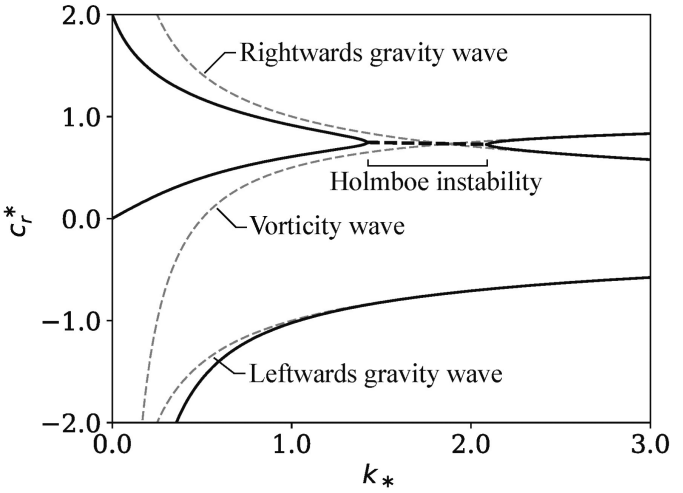

Figure 4.12 Dispersion relation of the Holmboe instability at $Ri_b = 2$. The black curves show $c_r^\star$ of the stable waves that exist in the Holmboe dispersion relation (4.36), and the black dashed line the region of the Holmboe instability. Gray dashed lines are the phase speeds of the isolated waves as labeled.

speeds of each of these modes in isolation (i.e., neglecting any interaction) follows from the jump condition (4.31):

$$\text{Vorticity wave:} \quad c = u_0 + \frac{\Delta Q_1}{2k} \quad \Rightarrow \quad c_\star = 1 - \frac{1}{2k_\star} \tag{4.37}$$

and

$$\text{Gravity waves:} \quad c = \pm\left(\frac{\Delta b}{2k}\right)^{1/2} \quad \Rightarrow \quad c_\star = \pm\left(\frac{Ri_b}{2k_\star}\right)^{1/2} \tag{4.38}$$

(cf. 2.44 and 3.81). These phase speeds are plotted in Figure 4.12 as dashed lines. They generally correspond closely to the modes seen in the full Holmboe dispersion relation. The correspondence is inexact, however, due to the interaction between the waves, which is stronger at lower $k_\star$ because the eigenfunctions extend further in the vertical (4.29).

In a mechanism identical to the resonance of two vorticity waves in the piecewise shear layer, the Holmboe instability arises from a resonance of the vorticity wave at $z = h$ and one of the internal gravity waves at $z = 0$. The interaction is centered around the crossing of the waves in the dispersion relation where there is a natural phase-locking, and can clearly be seen in Figure 4.12. This also suggests that we can approximate the location of the band of instability in the Ri_b-$k_\star$ plane by simply equating the speed of the rightward propagating internal gravity wave and the vorticity wave, giving

https://doi.org/10.1017/9781108640084.005 Published online by Cambridge University Press

$$Ri_b = 2k_\star\left(1 - \frac{1}{2k_\star}\right)^2. \tag{4.39}$$

This curve is plotted in Figure 4.11 and is clearly centered on the band of instability. Referred to as the resonance approximation, this technique is generally useful in identifying the wave resonances responsible for instability, especially in profiles with many possible interactions (Caulfield, 1994).

Finally, this case demonstrates that Rayleigh's inflection point theorem, and others from homogeneous flows, are no longer strictly accurate when stratification is present. In fact, we have seen that no inflection point is needed; stratification can in some sense "complete the inflection point" by providing the necessary wave resonance.

4.6.4 Multi-Layered Shear Flow: the Taylor-Caulfield Instability

Our final example involves no vorticity waves at all, but instead two interfacial gravity waves in a non-inflectional shear flow that resonate just as do the vorticity waves in section 3.12. The role of the shear is to facilitate phase-locking so that the resonance is sustained.

The background state has a three-layered stratification profile (Figure 4.13) with equal buoyancy jumps b_0 across interfaces located at $z = \pm h$. The background velocity is $u_0 z/h$, so the shear is uniform. The dispersion relation is found by applying the jump condition (4.31) at the interfaces:

$$c^4 - 2(u_0^2 + c_g^2)c^2 + (u_0^2 - c_g^2)^2 - e^{-4kh}c_g^4 = 0, \tag{4.40}$$

with $c_g = \sqrt{b_0/2k}$ as in the previous examples.

The stability diagram (Figure 4.13b) shows a band of instability with growth rates increasing with Ri_b up to $Ri_b = 1$. The instability, called the Taylor-Caulfield instability, is stationary with $c_r = 0$.

Here we have another example of statically stable stratification destabilizing a flow that is stable in the homogeneous case $Ri_b = 0$. The origin of the instability is in the resonance of the leftward propagating gravity wave at the upper interface with the rightward propagating gravity wave at the lower interface. The shear makes it possible for these waves to phase-lock. The phase-locking condition, corresponding to the crossing of the phase-speed curves in the dispersion diagram, can be found by setting the speeds equal to each other, giving[2] $Ri_b = 2k_\star$. This is again found to closely follow the band of instability in Figure 4.13.

[2] Try to derive this yourself. Be careful to include the speed of the mean flow at each buoyancy interface.

https://doi.org/10.1017/9781108640084.005 Published online by Cambridge University Press

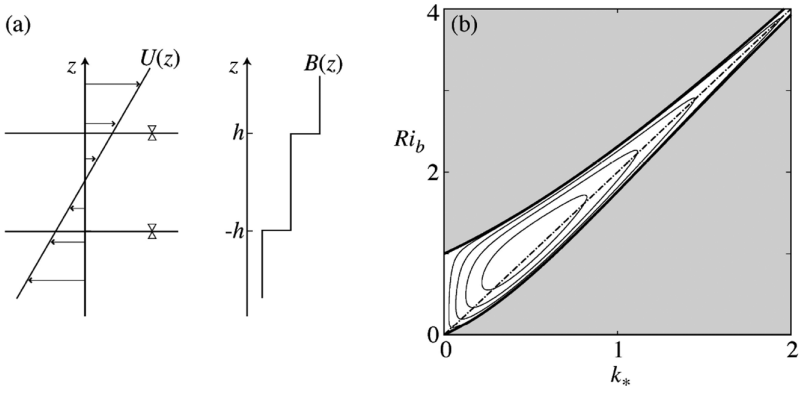

Figure 4.13 (a) Profiles illustrating the simplified setup for the Taylor-Caulfield instability of a sheared multilayered stratification. (b) Stability characteristics of the Taylor-Caulfield instability. Solid contours are of growth rate (every $0.02u_0/h$) with gray representing stable regions of propagating waves. All unstable modes are stationary with $c_r = 0$. Adapted from Carpenter et al. (2013).

4.7 The Miles-Howard Theorem

As we have discussed, the Richardson number $Ri = B_z/U_z^2$ quantifies the competing effects of stratification and shear. If $Ri \gg 1$, stratification dominates and the flow is stable. Conversely, if $Ri \ll 1$, instability is likely. The boundary between stable and unstable flows must lie at some intermediate value of Ri, which we'll call Ri_c. The Miles-Howard theorem tells us that the minimum of $Ri(z)$ must be less than $Ri_c = 1/4$ for instability to be possible. To be precise:

Miles-Howard theorem: *A necessary condition for instability in an inviscid, nondiffusive, stratified, parallel shear flow is that the minimum value of $Ri(z)$ be less than 1/4.*

To prove this, we transform the TG equation via the following change of variables:

$$\hat{w} = (U - c)^{1/2}\phi.$$

The algebra is left as an exercise; the result is:

$$\left[(U - c)\phi_z\right]_z + P(z)\phi = 0, \tag{4.41}$$

where

$$P = \frac{B_z - \frac{1}{4}U_z^2}{U - c} - \frac{1}{2}U_{zz} - k^2(U - c).$$

We now multiply (4.41) by ϕ^* and integrate over the vertical domain:

https://doi.org/10.1017/9781108640084.005 Published online by Cambridge University Press

$$\int_{z_B}^{z_T} \phi^* \big[(U-c)\phi_z\big]_z dz + \int_{z_B}^{z_T} \phi^* P(z)\phi dz = 0,$$

where z_B and z_T may be finite or infinite. Now integrate the first term by parts:

$$\phi^*(U-c)\phi_z\Big|_{z_B}^{z_T} - \int_{z_B}^{z_T} \phi_z^*(U-c)\phi_z dz + \int_{z_B}^{z_T} \phi^* P(z)\phi dz = 0.$$

Because $\hat{w}$ vanishes at the boundaries, the first term drops out and we have

$$-\int_{z_B}^{z_T} (U-c)|\phi_z|^2 dz + \int_{z_B}^{z_T} P(z)|\phi|^2 dz = 0.$$

The imaginary part is

$$c_i \int_{z_B}^{z_T} \left[|\phi_z|^2 + \frac{B_z - \frac{1}{4}U_z^2}{|U-c|^2}|\phi|^2 + k^2|\phi|^2 \right] dz = 0.$$

The first and third terms in the integrand are positive definite. Now suppose that the second term is also positive definite. In that case, the integral is positive, and the equation can only be satisfied if $c_i = 0$. Conversely, the only way c_i can be nonzero is if the second term is negative somewhere, i.e.,

$$B_z - \frac{1}{4}U_z^2 < 0\,, \quad \text{or} \quad Ri < 1/4,$$

for some z.

It is important to understand just what the Miles-Howard theorem does, and does not, say about the stability of particular profiles $U(z)$ and $B(z)$. Because it is a *necessary* condition for instability, it tells us only that instability is *possible* when $Ri < 1/4$ for some z, not that it actually occurs. In logical terms, what's proven is that *if* $c_i \neq 0$ *then* $Ri < 1/4$ for some z, not the converse. In practice, if we find that $Ri(z) < 1/4$ at some location and want to know whether instability is present, we must solve the Taylor-Goldstein equation explicitly. On the other hand, the theorem *does* definitively identify states where instability is *not* possible. If $Ri(z) > 1/4$ everywhere, no further analysis is needed; the flow is stable.

We have already seen the example of the continuously stratified shear layer (4.19), where instability requires that the minimum Ri be less than 0.25, consistent with the Miles-Howard theorem. As a second example, suppose the stratification is again $B^\star = Ri_b \tanh z^\star$, but the velocity profile is the Bickley jet $U^\star = \mathrm{sech}^2 z^\star$ as described in section 3.9.2. In this case, instability occurs if and only if the minimum Richardson number is less than 0.231 (Drazin and Howard, 1966; Hazel, 1972), again consistent with the theorem.

The examples shown in sections 4.6.2–4.6.4 are a different matter. At first glance, these appear to contradict the Miles-Howard theorem by exhibiting instability when $Ri_b > 0.25$. The contradiction is resolved by noting that, for these

https://doi.org/10.1017/9781108640084.005 Published online by Cambridge University Press

profiles, Ri_b is not the *minimum* value of $Ri(z)$. In fact, $Ri = 0$ for all z except at buoyancy interfaces, regardless of Ri_b. The theorem is therefore irrelevant for these simple models.

In a compressible fluid, the Miles-Howard theorem remains valid provided that B_z is calculated as in (2.64) and (2.65) as shown by Chimonas (1970).

4.8 Howard's Semicircle Theorem

The Miles-Howard theorem described in the previous section provides a condition that the *mean flow* must satisfy if instability is to grow. Here we describe a condition that the *mode* must satisfy.

Howard's semicircle theorem: *In an inviscid, nondiffusive, stably stratified, parallel shear flow, let the background velocity $U(z)$ be bounded by U_{min} and U_{max}. Any unstable normal mode must have complex phase speed c located within the semicircle centered at $c_r = (U_{max} + U_{min})/2, c_i = 0$ having radius $(U_{max} - U_{min})/2$, as shown on Figure 4.14.*

A corollary is that the real part c_r must lie within the range of the mean flow. In other words, every unstable mode must have a critical level. This result is a generalization of the critical level theorem (section 3.11.3).

The proof starts off similar to that for the Miles-Howard theorem (in fact it appeared in the same paper), but is more involved. We write the TG equation in terms of the vertical displacement, reproducing (4.21):

$$\left[(U-c)^2\hat{\eta}_z\right]_z + \left[B_z - k^2(U-c)^2\right]\hat{\eta} = 0 \tag{4.42}$$

(cf. exercise 9).

As before, we multiply by $\hat{\eta}^*$ and integrate over the vertical domain. Integrating by parts, using the boundary condition $\hat{\eta} \to 0$, and rearranging we obtain

$$\int_{z_B}^{z_T} B_z|\hat{\eta}|^2 dz = \int_{z_B}^{z_T} (U-c)^2\left[|\hat{\eta}_z|^2 + k^2(U-c)^2|\hat{\eta}|^2\right]dz. \tag{4.43}$$

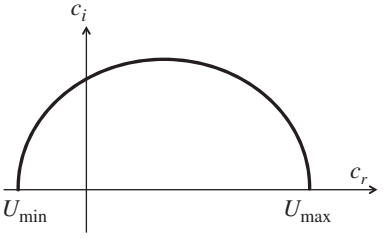

Figure 4.14 Howard's semicircle on the complex c-plane, bounded by the extremal values of the mean velocity. The phase speed of an unstable mode must lie within the semicircle (Howard, 1961).

https://doi.org/10.1017/9781108640084.005 Published online by Cambridge University Press

The imaginary part is

$$0 = -2c_i \int_{z_B}^{z_T} (U - c_r)\left[|\hat{\eta}_z|^2 + k^2|\hat{\eta}|^2\right]dz. \tag{4.44}$$

Because the quantity in square brackets is positive definite, the integral can be zero only if $U - c_r$ changes sign. Two implications of this are worth noting:

- The discussion so far is identical to our earlier proof that an unstable mode must have a critical level in a *homogeneous* shear flow (section 3.11.3). We now see that a critical level is also necessary in *stratified* flow. The stratification term on the left-hand side of (4.43) becomes irrelevant when we take the imaginary part.
- In the special case $U = 0$, this result shows that c_r must be zero. This is relevant to the convective case $B_z < 0$, which we examined in section 2.2.3. We see once again that all unstable modes are stationary.

To extend the proof, we now consider the real part of (4.43):

$$\int_{z_B}^{z_T} B_z|\hat{\eta}|^2 dz = \int_{z_B}^{z_T} (U^2 - 2c_r U + c_r^2 - c_i^2)\left[|\hat{\eta}_z|^2 + k^2|\hat{\eta}|^2\right]dz. \tag{4.45}$$

The second term on the right-hand side can be written as

$$-2c_r \int_{z_B}^{z_T} U\left[|\hat{\eta}_z|^2 + k^2|\hat{\eta}|^2\right]dz$$

which, by (4.44), is equal to

$$-2c_r \int_{z_B}^{z_T} c_r\left[|\hat{\eta}_z|^2 + k^2|\hat{\eta}|^2\right]dz.$$

Therefore, in the second term on the right-hand side of (4.45), we can change the U to c_r, resulting in

$$\int_{z_B}^{z_T} B_z|\hat{\eta}|^2 dz = \int_{z_B}^{z_T} (U^2 - |c|^2)\left[|\hat{\eta}_z|^2 + k^2|\hat{\eta}|^2\right]dz. \tag{4.46}$$

If $B_z > 0$, we have

$$\int_{z_B}^{z_T} (U^2 - |c|^2)\left[|\hat{\eta}_z|^2 + k^2|\hat{\eta}|^2\right]dz > 0. \tag{4.47}$$

Now comes the cute part. Define U_{max} and U_{min} as the maximum and minimum values of $U(z)$. Note that $U_{max} - U \geq 0$ and $U_{min} - U \leq 0$, and therefore

$$(U_{max} - U)(U_{min} - U) \leq 0.$$

As a result,

$$\int_{z_B}^{z_T} (U_{max} - U)(U_{min} - U)\left[|\hat{\eta}_z|^2 + k^2|\hat{\eta}|^2\right]dz \leq 0,$$

https://doi.org/10.1017/9781108640084.005 Published online by Cambridge University Press

or

$$\int_{z_B}^{z_T} \left[U_{max}U_{min} - U(U_{max} + U_{min}) + U^2\right]\left[|\hat{\eta}_z|^2 + k^2|\hat{\eta}|^2\right]dz \leq 0. \tag{4.48}$$

Note that the integrand is the product of the two factors in square brackets. We will now convert the first of these factors to a constant, which we can then remove from the integral. We do this in two steps. First, as we noted above, (4.44) allows us to replace U with c_r in the second term. Now consider the third term, which contains U^2. By (4.47),

$$\int_{z_B}^{z_T} |c|^2\left[|\hat{\eta}_z|^2 + k^2|\hat{\eta}|^2\right]dz < \int_{z_B}^{z_T} U^2\left[|\hat{\eta}_z|^2 + k^2|\hat{\eta}|^2\right]dz.$$

So if we replace U^2 by $|c|^2$ in (4.48), the inequality is still true:

$$\int_{z_B}^{z_T} \left[U_{max}U_{min} - c_r(U_{max} + U_{min}) + |c|^2\right]\left[|\hat{\eta}_z|^2 + k^2|\hat{\eta}|^2\right]dz \leq 0. \tag{4.49}$$

Given that the first factor in the integrand is a constant and the second is positive definite, the inequality can be true only if the first factor is negative:

$$U_{max}U_{min} - c_r(U_{max} + U_{min}) + |c|^2 \leq 0.$$

After some juggling, this becomes

$$\left(c_r - \frac{U_{max} + U_{min}}{2}\right)^2 + c_i^2 \leq \left(\frac{U_{max} - U_{min}}{2}\right)^2. \tag{4.50}$$

This inequality describes the interior of a circle on the complex c-plane whose radius is $(U_{max} - U_{min})/2$ and whose center is on the real axis at $(U_{max} + U_{min})/2$. For any unstable mode, $c_i > 0$ and therefore c must lie in the upper half of the circle; i.e., in Howard's semicircle, as shown in Figure 4.14.

Note that, like the Miles-Howard theorem, the semicircle theorem is a statement that *if* there is an unstable mode, *then* certain conditions are true, not the other way around. A mode can lie within the semicircle and still not be unstable.

4.9 Energetics

To analyze the perturbation kinetic energy, we repeat the calculation of section 3.10, beginning with the momentum equation (4.8) instead of (3.7). The only difference is the buoyancy term $b'\hat{e}^{(z)}$. Therefore, converting to normal mode form gives the same results for the continuity and horizontal momentum equations but the vertical momentum equation now contains the normal mode buoyancy perturbation $\hat{b}$:

$$(\sigma + \imath kU)\,\hat{w} = -\hat{\pi}_z + \hat{b}. \tag{4.51}$$

https://doi.org/10.1017/9781108640084.005 Published online by Cambridge University Press

As in section 3.10, we multiply the momentum equations by the conjugates of the velocity eigenfunctions, take the real part, and divide by 2. The result is (3.64) with an added term:

$$\boxed{2\sigma_r K = SP - \frac{d}{dz} EF + BF,} \tag{4.52}$$

where

$$BF = \overline{w'b'} = \frac{1}{2}(\hat{w}^* \hat{b})_r$$

is the buoyancy flux, also called the buoyancy production. As before, the overbar represents a horizontal average over an integer number of wavelengths.

When buoyant fluid rises and dense fluid sinks, $BF > 0$. Therefore, BF is the second term we have found (after SP) that is capable of creating kinetic energy.[3] This term is the source of kinetic energy for convective instability. In contrast $BF < 0$ means that the instability has to do work against gravity in order to grow, i.e., it must lift dense fluid and depress buoyant fluid. Like the shear production (and unlike the energy flux), the buoyancy production can integrate to a nonzero value, and can therefore increase or decrease the net kinetic energy of a disturbance. It is often useful to classify instabilities according to whether their main energy source is SP or BF (Table 4.1).

The buoyancy flux also shows up in the buoyancy variance budget. To derive this budget, we start with (4.15), the buoyancy perturbation equation in normal mode form:

$$(\sigma + \imath k U)\hat{b} + B_z \hat{w} = 0.$$

By analogy with the development of the kinetic energy equation, we multiply through by $\hat{b}^*$, take the real part, and divide by 2. The result is

$$\sigma_r \frac{|\hat{b}|^2}{2} = -\frac{B_z}{2}(\hat{b}^* \hat{w})_r = -B_z \, BF.$$

The only source of buoyancy variance is a production term that quantifies the interaction of B_z and BF.

A mode can grow only if B_z and BF have opposite sign. In the case of statically stable stratification, $B_z > 0$ and therefore $BF < 0$. Referring back to the kinetic energy budget (4.52) we see that, when $B_z > 0$, the buoyancy flux can *only* act to reduce growth, just as we surmised in section 4.1.

Now here is a paradox. In some cases (e.g., Holmboe instability), growth is possible *only* in the presence of stable stratification, even though the resulting

[3] More precisely, it converts potential energy into kinetic energy.

https://doi.org/10.1017/9781108640084.005 Published online by Cambridge University Press

Table 4.1 *Categorizing instabilities by their energy source.*

	$BF < 0$	$BF > 0$
$SP < 0$	stable	convective instability opposed by shear
$SP > 0$	shear instability opposed by buoyancy	sheared convection

buoyancy flux can *only* act to reduce growth. The resolution of this paradox is that, even though some kinetic energy is diverted through BF, the stable stratification causes the velocity field to arrange itself such that the *shear production* SP is positive. Specifically, the resonance between the phase-locked shear and gravity waves causes the phase lines of w' to tilt against the shear as in section 3.11.4. Thus, *while shear is the energy source for the instability, it is buoyancy that allows that energy source to be tapped.*

4.10 Summary

For a parallel shear flow $U(z)$ in an inviscid, nondiffusive fluid with density stratification described by $B(z)$, the following are true:

- The gradient Richardson number $Ri = B_z/U_z^2$ compares the effects of stratification and shear.
- The Taylor-Goldstein equation (4.18) describes a wide array of instabilities and wavelike phenomena.
- A normal mode disturbance is affected only by that component of the background flow that is parallel to its own wave vector.
- Instability is possible only if $Ri(z) < 1/4$ for some z (the Miles-Howard theorem).
- The complex phase speed of a growing mode must lie within the semicircle shown in Figure 4.14 (Howard's semicircle theorem).
- The rule of thumb for a shear layer, i.e., that the wavelength is 7 times the layer thickness, remains valid in the stratified case.

4.11 Further Reading

Miles (1961) is an immense work that covered considerable new ground before arriving at the proof of what we now call the Miles-Howard theorem (section 4.7). That paper was sent to L. Howard for peer review, whereupon Howard discovered the much simpler proof reproduced here (Howard, 1961). For good measure, Howard also proved the semicircle theorem (section 4.8).

See Smyth and Moum (2012) for more information on Kelvin-Helmholtz instability. A review of wave resonance in stratified shear flows is provided in

https://doi.org/10.1017/9781108640084.005 Published online by Cambridge University Press

Carpenter et al. (2013), as well as nice descriptions in Baines and Mitsudera (1994) and Caulfield (1994). It is also worth consulting Holmboe (1962), where it all began.

4.12 Appendix: Veering Flows

In many important cases, the mean flow varies primarily with height, but is not parallel. In an Ekman spiral, for example, both speed and direction change with height. Equatorial mean currents are mostly zonal, but these are exceptional. In most parts of the ocean and atmosphere, the mean current veers with depth.

Happily, the theory that we have already developed for parallel flows is easily extended to veering flows using our results from section 4.3 above: an instability is affected by only the component of the mean flow parallel to its own wave vector, and that component is a parallel shear flow.

Suppose that the mean flow of interest varies in z but has components in both horizontal directions:

$$\vec{u} = U(z)\hat{e}^{(x)} + V(z)\hat{e}^{(y)}.$$

For a given wave vector (k, ℓ), we define the parallel component of the mean flow:

$$\boxed{\tilde{U}(z) = \frac{kU(z) + \ell V(z)}{\tilde{k}}.}$$

Everything we have learned in this chapter about parallel flows is also true for veering flows if we substitute $\tilde{U}$ for U in (4.14) and (4.15).

4.13 Appendix: Spatial Growth

Throughout this book we separate the linearized equations of motion using normal modes in which the dependences on the horizontal coordinates and time take forms like

$$e^{\imath kx+\sigma t}, \quad e^{\imath(kx-\omega t)}, \quad \text{or } e^{\imath k(x-ct)}. \tag{4.53}$$

(We restrict this discussion to 2D modes.) In all cases, we assume that the wavenumber k is purely real, so that the solution is horizontally periodic. Time dependence is then quantified by the complex eigenvalue σ, or ω, or c.

The assumption of horizontal periodicity is not always realistic. Consider, for example, two streams, moving at different speeds, that meet at some point in space (e.g., Figure 4.15). Shear instability grows not in time but rather in the downstream direction, beginning at the point of confluence. In this case, a more realistic assumption is that ω is real (or, equivalently, σ is imaginary) and the streamwise

https://doi.org/10.1017/9781108640084.005 Published online by Cambridge University Press

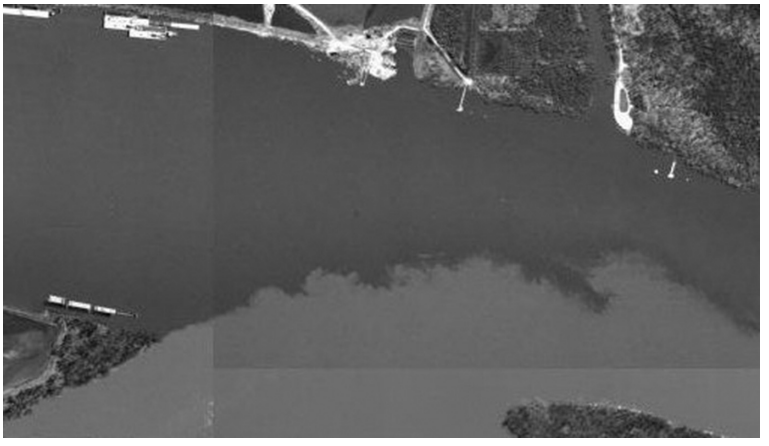

Figure 4.15 Confluence of the silty Missouri and clearer Mississippi rivers near St. Louis, MO, showing spatially growing instability. Image courtesy United States Geological Survey (USGS).

wavenumber k is allowed to be complex. The imaginary part of k then quantifies the rate of downstream growth.

As a simple model, consider the single interface that we explored in section 4.6.1. Assuming that the streams are side-by-side as in Figure 4.15, we can simplify further by neglecting the buoyancy force, so that the dispersion relation (4.25) becomes

$$\left(\frac{u_0}{2} - c\right)^2 + \left(-\frac{u_0}{2} - c\right)^2 = 0.$$

Solving for c, we get a purely imaginary result:

$$c = \pm\imath\frac{u_0}{2}.$$

In this model the streams have mean speeds $\pm u_0/2$. The scene is easier to imagine if we choose coordinates so that one stream is stationary while the other has speed u_0, which simply requires adding $u_0/2$ to all velocities. In this new reference frame,

$$c = \frac{u_0}{2}(1 \pm \imath).$$

So the real part of the phase velocity is, not surprisingly, the average of the speeds of the two streams. Now $c = \omega/k$, so we can easily solve for k:

$$k = \frac{\omega}{u_0}(1 \pm \imath).$$

Referring back to (4.53) and assuming that ω is real, we can see that the solution for k with the minus sign describes exponential growth in x. The wavelength is

https://doi.org/10.1017/9781108640084.005 Published online by Cambridge University Press

$2\pi u_0/\omega$, and the growth rate is such that the amplitude grows by a factor $e^{2\pi} = 535$ over that distance!

Both wavenumber and spatial growth rate are proportional to the frequency ω, which is not specified. In reality, billows form quickly at extremely small scales, then merge repeatedly to form the large billows you see in Figure 4.15. The process is essentially chaotic; all that can be predicted reliably is the phase speed. There is much more that could be said regarding spatially growing instabilities that we will not cover in this book. For more details we refer the interested reader to the overview by Huerre (2000).

Exercise: Repeat this calculation with $b_0 \neq 0$, representing streams of different density separated by a horizontal boundary, as in section 4.6.1. You should find that there is a minimum frequency below which spatial instability does not occur.

https://doi.org/10.1017/9781108640084.005 Published online by Cambridge University Press